Perturbation theory remixed: Improved nonlinearity modeling beyond standard perturbation theory

Zhenyuan Wang (王震远),[1] Donghui Jeong,[1,2] Atsushi Taruya,[3,4] Takahiro Nishimichi,[3,4,5] and Ken Osato[6,7,3]

[1]*Department of Astronomy and Astrophysics and Institute for Gravitation and the Cosmos, The Pennsylvania State University, University Park, Pennsylvania 16802, USA*
[2]*School of Physics, Korea Institute for Advanced Study, Seoul, South Korea*
[3]*Center for Gravitational Physics and Quantum Information, Yukawa Institute for Theoretical Physics, Kyoto University, Kyoto 606-8502, Japan*
[4]*Kavli Institute for the Physics and Mathematics of the Universe, Todai Institutes for Advanced Study, The University of Tokyo, Kashiwa, Chiba 277-8583, Japan*
[5]*Department of Astrophysics and Atmospheric Sciences, Faculty of Science, Kyoto Sangyo University, Motoyama, Kamigamo, Kita-ku, Kyoto 603-8555, Japan*
[6]*Center for Frontier Science, Chiba University, Chiba 263-8522, Japan*
[7]*Department of Physics, Graduate School of Science, Chiba University, Chiba 263-8522, Japan*

(Received 7 September 2022; accepted 21 April 2023; published 31 May 2023)

We present a novel *n*EPT (*n*th-order Eulerian perturbation theory) scheme to model the nonlinear density field by the summation up to *n*th-order density fields in perturbation theory. The obtained analytical power spectrum shows excellent agreement with the results from all 20 Dark-Quest suites of *N*-body simulations spreading over a broad range of cosmologies. The agreement is much better than the conventional two-loop standard perturbation theory and would reach out to $k_{\rm max} \simeq 0.4\ h/{\rm Mpc}$ at $z = 3$ for the best-fitting *Planck* cosmology, without any free parameters. We find that the *n*EPT results, particularly for $n > 4$, depend sensitively on the grid size, but that can be removed by employing an effective field theory-type fitting function. The method can accelerate the forward modeling of the nonlinear cosmological density field, an indispensable probe of cosmic mysteries such as inflation, dark energy, and dark matter.

DOI: 10.1103/PhysRevD.107.103534

I. INTRODUCTION

The observations of the Universe's large-scale structure (LSS) traced by Cosmic Microwave Background (CMB) radiation [1,2], the distribution of galaxies [3–7], and shape distortion of galaxies [8,9] have led to the concordance ΛCDM cosmology [10] with most parameters measured to a subpercent accuracy.

Parallel to the data collection programs has been the theoretical development based upon which we interpret the observation. Starting from the 1940s [11], relativistic theory for the evolution of density perturbations in the Friedmann-Lemaître-Robertson-Walker universe has been developed and used to interpret the LSS data. In particular, its linearized version [12–14] has been so successful in explaining the power spectrum of CMB temperature anisotropies and polarizations to all scales observed by WMAP [15] and *Planck* [10] satellites. The concordance ΛCDM cosmology model would not be possible without such an accurate linear-theory model.

The remaining big questions in cosmology are to uncover the nature of building blocks of the ΛCDM cosmology, such as inflation, dark energy, and dark matter. To address these questions, modern galaxy surveys are mapping the distribution and shape distortion of galaxies with unprecedented depth and volume [16–22].

These observational developments call for a novel theoretical model beyond the linear theory that is only applicable on large scales where the accuracy of the usual LSS observation is limited by cosmic variance. Using a feature such as baryon acoustic oscillation (BAO) that is insensitive to the nonlinearities has proven successful for measuring the geometry of the Universe [23–25]. Upon modeling nonlinearities, however, using the full power-spectrum shape can improve the measurement accuracy by a factor of few [26,27]. In addition, the full-shape analysis enables the measurement of the growth rate of the LSS [28] and features in the galaxy clustering carved by massive neutrinos [29] and primordial physics [30].

A diversity of modeling methods have been developed ranging from simulation-based methods such as emulator [31–34], fast simulations [35–38], and machine learning [39,40] to analytical methods such as standard perturbation theory (SPT) [41,42], Lagrangian perturbation theory (LPT) [41,43,44], effective field theory of large scale structure (EFTofLSS) [45–47], and various renormalized perturbation theory (RPT) [48–59], including regularized perturbation theory (RegPT) [60,61].

Traditionally, the analytical methods focus on obtaining the expressions for the ensemble mean of the summary statistics such as the power spectrum and bispectrum, or n-point correlation functions. Such expressions usually involve high-dimensional integrals whose complexity increases quickly for the higher-order loop calculations. While Refs. [62–66] have developed fast methods for computing nonlinear power spectrum and bispectrum by using the FFTlog algorithm [67] or response function expansion [60,68], the analytical computation beyond the two-loop proves challenging [69].

The PT-based analytical methods can also be used to model the cosmic density field at the field level [70–77]. Instead of computing the ensemble mean of the summary statistics, the field-level computation provides nonlinear density fields from a given realization of the stochastic linear field. In this method, the computation of higher-order summary statistics is much easier than the analytical methods because we can simply take the average over the multiple realizations. For example, Ref. [74] shows that the field-level modeling provides a fast way to compute the summary statistics and their covariance matrices incorporating survey window function due to nontrivial geometry and varying depth. In addition, Ref. [77] presents the two-loop power spectrum and one-loop bispectrum of matter in redshift-space with this grid-based method. The possibility of field-level inference bypassing the summary statistics [78] further strengthens the motivation for the field-based method.

In this paper, we present a novel nEPT (nth-order Eulerian perturbation theory) scheme for modeling the nonlinear density field. For the field-level SPT calculation, we use the GridSPT [71] that, unlike LPT, directly generates the density and velocity fields on grids without using particles. While using the recursion relations of the SPT to compute nonlinear fields at each order, nEPT differs from the other PT methods in computing the summary statistics; namely, nEPT first adds all nonlinear contributions to the density field up to the nth order, then compute the summary statistics. By contrast, the SPT computes the summary statistics by collecting the contributions at fixed order in the linear density contrast $\delta_{\rm L}$.

In what follows, we show that nEPT models the nonlinear LSS with stunning accuracy, much better than the current state-of-the-art two-loop PT predictions.

II. GridSPT AND nEPT

For a given realization of the linear density field on regular grid points, the GridSPT [71] provides a way to compute the matter density field δ and the velocity field $\boldsymbol{v}$ of LSS perturbatively by solving the fluid equations,

$$\dot{\delta} + \nabla \cdot [(1+\delta)\boldsymbol{v}] = 0, \tag{1}$$

$$\dot{\boldsymbol{v}} + (\boldsymbol{v}\cdot\nabla)\boldsymbol{v} + \frac{\dot{a}}{a}\boldsymbol{v} = -\nabla\phi, \tag{2}$$

along with the Poisson equation,

$$\nabla^2\phi = 4\pi G\bar{\rho}_{\rm m}a^2\delta. \tag{3}$$

Here, dot represents the conformal-time derivative, $d\tau = dt/a$ with $a(t)$ being the scale factor and t being the cosmic time, ∇ is comoving-coordinate derivative, $\bar{\rho}_{\rm m}$ is the mean matter density, and ϕ is the peculiar gravitational potential. The set of equations describes the nonrelativistic-matter (cold-dark matter and baryon) fluid on scales larger than the baryonic Jeans scale. Following the standard practice of SPT, we assume irrotational velocity at all orders and expand the density field and the reduced velocity-divergence field $\theta \equiv -(\nabla\cdot\boldsymbol{v})/(aHf)$ as

$$\delta(\tau,\boldsymbol{x}) = \sum_n [D(\tau)]^n \delta^{(n)}(\boldsymbol{x}), \tag{4}$$

$$\theta(\tau,\boldsymbol{x}) = \sum_n [D(\tau)]^n \theta^{(n)}(\boldsymbol{x}). \tag{5}$$

Making use of the fast Fourier transform, the GridSPT enables us to quickly generate the nth order quantities $\delta^{(n)}$ and $\theta^{(n)}$ at each grid point following the configuration-space SPT recursion relation [71]. Here, D denotes the linear growth factor and $f \equiv d\ln D/d\ln a$.

The crucial difference between nEPT and the usual PT is that in nEPT, we first compute the nonlinear density field in Eq. (4) up to a fixed order n, then estimate the summary statistics, such as power spectrum and bispectrum, directly from δ. For example, for $n = 5$, the power spectrum from 5EPT reads

$$\begin{aligned} P_{\rm 5EPT} = {} & D^2P_{11} + 2D^3P_{12} + D^4(2P_{13}+2P_{22}) \\ & + D^5(2P_{14}+2P_{23}) + D^6(2P_{15}+2P_{24}+P_{33}) \\ & + D^7(2P_{25}+2P_{34}) + D^8(2P_{35}+P_{44}) \\ & + 2D^9P_{45} + D^{10}P_{55}, \end{aligned} \tag{6}$$

which clearly differs from the nonlinear power spectrum in the usual PT,

$$\begin{aligned} P_{\rm PT}^{(2-{\rm loop})} = {} & D^2P_{11} + D^4(2P_{13}+P_{22}) \\ & + D^6(2P_{15}+2P_{24}+P_{33}). \end{aligned} \tag{7}$$

Here, we use the shorthand notation of

$$\langle \delta^{(n)}(\boldsymbol{k})\delta^{(m)}(\boldsymbol{k}')\rangle \equiv (2\pi)^3 P_{nm}(k)\delta^D(\boldsymbol{k}+\boldsymbol{k}'), \tag{8}$$

and suppress the τ and k dependencies to avoid the clutter. The first (second) bracket in Eq. (7) is called one-loop (two-loop) contribution in SPT. Note that the odd-order components like P_{12}, P_{14}, P_{23}, etc., are neglected in usual PT because these components have zero-ensemble mean for our interest in the Gaussian initial condition. Although starting from the Gaussian initial condition, however, we

find that these odd-order terms add nonzero contributions to the power spectrum of a single realization, and adding them improves the matching between the PT prediction and the N-body results.

III. N-BODY SIMULATIONS

We test the performance of the nEPT modeling of the nonlinear power spectrum by comparing the nEPT prediction in Eq. (6) against a series of N-body simulations. First, we use the baseline N-body simulation in Ref. [71]; 1024^3 particles in $L_{\rm box} = 1\ {\rm Gpc}/h$ box with flat-ΛCDM cosmology ($\Omega_{\rm m} = 0.279$, $h = 0.701$, $n_s = 0.96$, $\sigma_8 = 0.8159$) consistent with WMAP 5-year results [79]. Then, we use the N-body simulation results from the Dark Quest project [80] aiming to model the cosmological dependence of halo and matter statistics in the six-parameter wCDM cosmologies. The 20 simulations are for the 20 test cosmologies arranged uniformly over the six-dimensional hyperrectangle, covering roughly up to a $\sim 10\sigma$ range of the 2015 Planck data [81] for a flat ΛCDM model around its central best-fitting model, based on a maxi-min distance Latin hypercube design. Specifically, the parameter range of wCDM cosmology is as follows:

$$\begin{aligned} &0.0211375 < \omega_{\rm b} < 0.0233625,\\ &0.10782 < \omega_{\rm c} < 0.13178,\\ &0.54752 < \Omega_{\rm de} < 0.82128,\\ &2.4752 < \ln(10^{10} A_s) < 3.7128,\\ &0.916275 < n_s < 1.012725,\\ &-1.2 < w < -0.8. \end{aligned} \tag{9}$$

In particular, we use the high-resolution suite with 2048^3 mass elements in $(1\ {\rm Gpc}/h)^3$ periodic comoving boxes. For both cases, we measure the matter power spectrum employing 1024^3 grid points for FFT, with the aliasing artifact and the cloud-in-cells mass assignment kernel corrected in Fourier space [82,83]. The measurement error is much less than 1% up to the Nyquist frequency of $k = 3.2\ h/{\rm Mpc}$.

IV. $P(k)$ COMPARISON: nEPT vs N-BODY

To make a face-to-face comparison with the N-body results, we calculate the GridSPT nonlinear density field using the same initial linear density field that generates the initial condition for corresponding N-body simulations.

When computing the Fourier-space quantities using real-space recursion relations, one must apply the cutoff to reduce the spurious impact from the small-scale (UV) modes. For the baseline calculation, we use the cutoff wave number $k_{\rm cut}^{\rm UV} = 256 k_F = 1.61\ h/{\rm Mpc}$, but we shall also present the results with different $k_{\rm cut}$ later. Here, $k_F = 2\pi/L_{\rm box}$ is the fundamental wave number. To avoid the aliasing effect, we adopt the generalized Orszag rule [75,77] to zero-pad $k > 2/(n+1)k_{\rm Nyquist}$ in linear density field for computing the nth order field, where $k_{\rm Nyquist} = \pi N_{\rm grid}/L_{\rm box}$ is the Nyquist wavenumber with the one-dimensional grid size $N_{\rm grid}$. Requiring that $k_{\rm cut}^{\rm UV} < 2/(n+1)k_{\rm Nyquist}$ sets the minimum $N_{\rm grid}$ that we use for the GridSPT calculation. For the baseline computation, we use $N_{\rm grid} = 1536$.

We have computed up to fifth-order GridSPT density fields that are sufficient for calculating SPT power spectrum to two-loop level and 5EPT by using, respectively, Eq. (6) and Eq. (7). Figure 1 shows the ratios of various model nonlinear power spectra to the baseline N-body power spectrum at the following six redshifts: $z = 0$, 0.5, 1, 2, 3, and 5. Models plotted here are SPT (dashed lines), nEPT (thick solid lines), RegPT+ (thin brown line [61]), and IR-resummed EFT (thin olive line [61]). To facilitate the comparison, we highlight the one- and two-percentage ranges by yellow and lavender bands at the center and extend the three high-redshift (right) panels to $k = 0.8\ h/{\rm Mpc}$.

First, we note that the agreement between nEPT and N-body improves significantly as n increases for $z \gtrsim 0.5$, and the 5EPT (the cyan lines) agrees with N-body results better than one percent to larger wave number than two-loop SPT $P(k,z)$ for $z \gtrsim 1$. Such accuracy of 5EPT can only be matched with two-loop results of the RegPT+ and IR-resummed EFT that employ, respectively, one and three free parameters. Here, we show the RegPT+ and IR-resummed EFT to the maximum wave number minimizing the reduced χ^2 assuming the diagonal covariance matrix with $\sigma[P(k)] = P(k)/\sqrt{N_k}$ [84]. Note that for RegPT+ with $z \le 3$, we find $k_{\rm max} = 0.25\ h/{\rm Mpc}$. It is worth reminding the readers that the nEPT scheme itself requires no free parameters. Later in this paper, we show that the result depends on the grid size, particularly for $n > 4$, but the grid-size dependence can be removed by adding EFT-type fitting parameters.

The nEPT and SPT results are also much smoother than the RegPT+ and IR-resummed EFT results. This is because the latter two models are the ensemble averages while nEPT and SPT are computed with the input linear density field of the N-body. In addition, we have added the odd-order terms (with odd power of D in Eq. (6)) to one-loop and two-loop power spectra. Although much smaller than the even-power terms, these odd-power terms indeed make the power spectrum from the same realization closer to the N-body result [71,85], especially for the large-scale Fourier modes [77].

We note that, at $z > 0.5$ where nEPT improves the agreement, nEPT does not *suffer* from the poor convergence in SPT whose residual shows alternating-series-like behavior, which motivates the development of renormalized PT [48]. Instead, below the wave number that nEPT starts to diverge, the agreement between nEPT and N-body

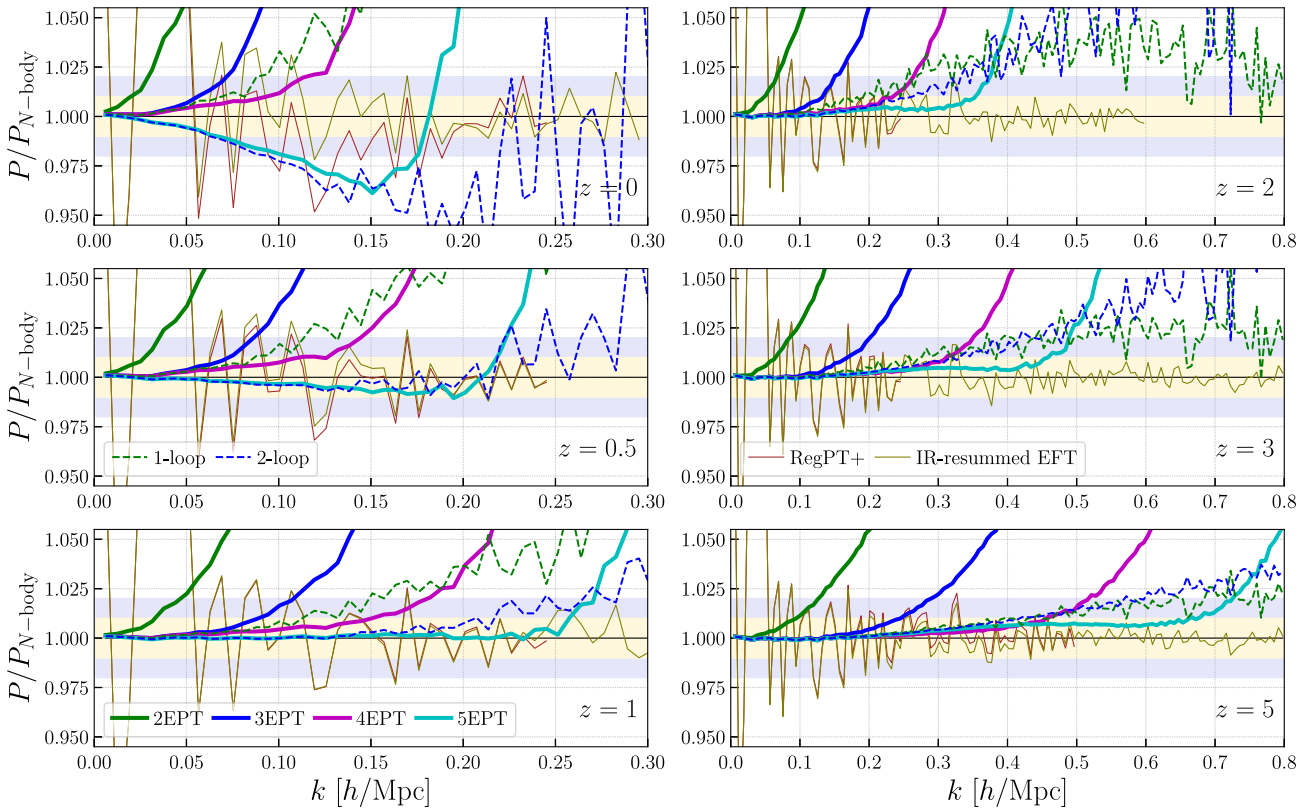

FIG. 1. The ratios of the model power spectra to the N-body results for the baseline WMAP-5yr cosmology at redshifts $z = 0, 0.5, 1, 2, 3$, and 5. The thin dashed lines are the one-loop (green), and two-loop (blue) power spectra from SPT calculations. The thick solid lines are the result from nEPT calculations: 2EPT (green), 3EPT (blue), 4EPT (magenta) and 5EPT (cyan). Both SPT and nEPT results are measured from the density field in GridSPT using the same initial linear density field generating the initial condition of the N-body simulation. The two thin solid lines are the two-loop results of RegPT+ (brown) and IR-resummed EFT (olive) using the smooth (theory) linear power spectrum. The yellow and lavender bands indicate the $\pm 1\%$ and $\pm 2\%$ regions. We truncated RegPT+ and IR-resummed EFT beyond the k_{max} that gives rise to the minimum reduced χ^2.

simulation is steadily improving as the order n increases. Also, nEPT enjoys well-regulated high-k behavior from the fact that contributions coming from higher order are stiffer by a factor of k^2, as we show in Fig. 2.

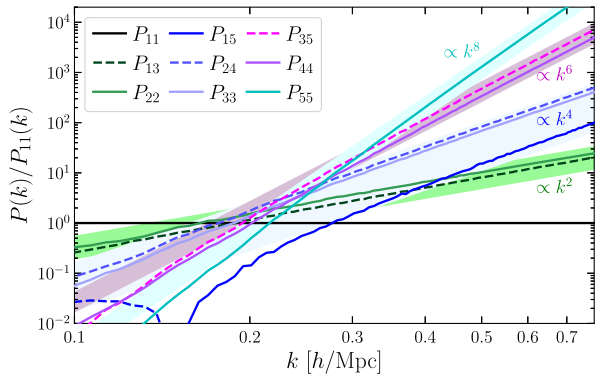

FIG. 2. The ratios of even-order components $P_{nm}(k)$ to the linear power spectrum. Solid (Dashed) lines denote positive (negative) values, and the components of the same order are plotted with similar colors. The shaded regions show the power law: k^2 (green), k^4 (blue), k^6 (magenta), and k^8 (cyan).

Finally, one noteworthy feature in Fig. 1 is that no wiggling feature appears in the ratio between nEPT and N-body around the BAO scales, which means that the damping of BAO has been accurately captured by nEPT, and the IR-resummation [86,87] might not be necessary for nEPT.

We confirm that the same conclusion also holds for cosmological models different from the WMAP-5yr cosmology by comparing the nEPT results to the outcome from 20 Dark Quest simulations, at 21 redshifts from $z = 0$ to 1.48. Furthermore, we find that the k_{max}, maximum wave number below which nEPT models the N-body result to one-percent accuracy, depends primarily on the $\sigma_8(z) = \sigma_8 D(z)$ value at the redshift. The top panel of Fig. 3 shows four representative results with different $\sigma_8(z)$, and the left panel of Fig. 4 shows the k_{max} measured from nEPT as a function of $\sigma_8(z)$.

Here, we test the effect of the UV cutoff by calculating the nEPT power spectra with two other UV cutoffs, $(k^{\mathrm{UV}}_{\mathrm{cut},1}, k^{\mathrm{UV}}_{\mathrm{cut},2}) = (200, 340)k_F = (1.26, 2.14)\ h/\mathrm{Mpc}$, and show the result as shaded regions in Fig. 3, and as ranges in Fig. 4. As expected, the higher-order nEPT is much more sensitive to the UV cutoff than the lower-order

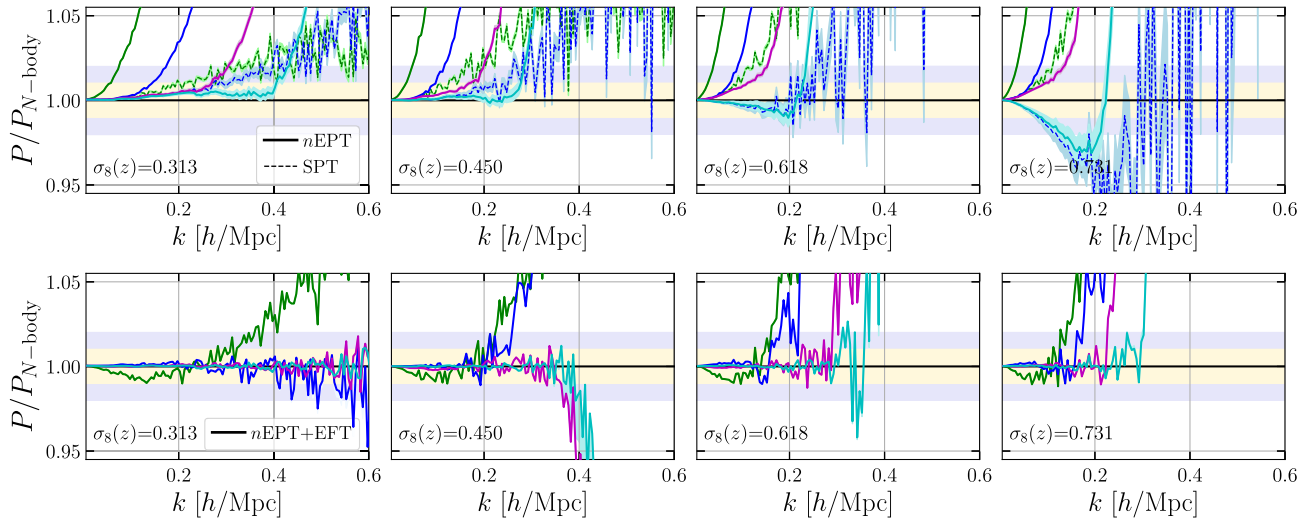

FIG. 3. (*Top*) The ratios of the real-space power spectra from *n*EPT (solid lines) and SPT (dashed lines) to the *N*-body results in four representative Dark Quest cosmologies. The colors are the same as that in Fig. 1. The shades show the range of *n*EPT power spectrum with different $k_{\rm cut}^{\rm UV}$ between 1.26 h/Mpc and 2.14 h/Mpc. (*Lower*) The same as the Top panel but for the *n*EPT power spectrum with EFT correction in Eq. (10).

*n*EPT. Although going to 5EPT can significantly improve the accuracy of modeling the nonlinearities in matter clustering, for example, 5EPT is accurate up to $k_{\rm max} = 0.35(0.40)$ h/Mpc at redshift $z = 2(3)$ in *Planck* cosmology (dashed vertical lines in Fig. 4), one must be cautious on the UV sensitivity.

The UV-cutoff dependence of *n*EPT, however, can be absorbed into the EFT-like counterterms. Motivated by Fig. 2, we have included the EFT correction as

$$\tilde{P}_{n\rm EPT}(k) = P_{n\rm EPT}(k) - \sum_{i=1}^{n-1} \alpha_i k^{2i} P_{11}(k), \qquad (10)$$

where P_{11} is the linear power spectrum of the *N*-body simulation, and $\{\alpha_i\}$ are free parameters that we fit from the measured power spectrum. As we have done for the RegPT+ and IR-resummed EFT, we find the $k_{\rm max}$ at which $\tilde{P}_{n\rm EPT}(k)$ proivdes the best fit to the *N*-body results. The shades in the lower panel of Fig. 3 and the ranges in the right panel of Fig. 4 are too narrow to be identified, which indicates that the EFT counterterms in Eq. (10) absorb the UV sensitivity in *n*EPT. Furthermore, as shown in the right panel of Fig. 4, the EFT correction improves the $k_{\rm max}$ of all *n*EPT power spectra significantly, especially at low $\sigma_8(z)$. For instance, with EFT correction, 5EPT can work accurately up to $k_{\rm max} = 0.6$ h/Mpc at $z = 2$.

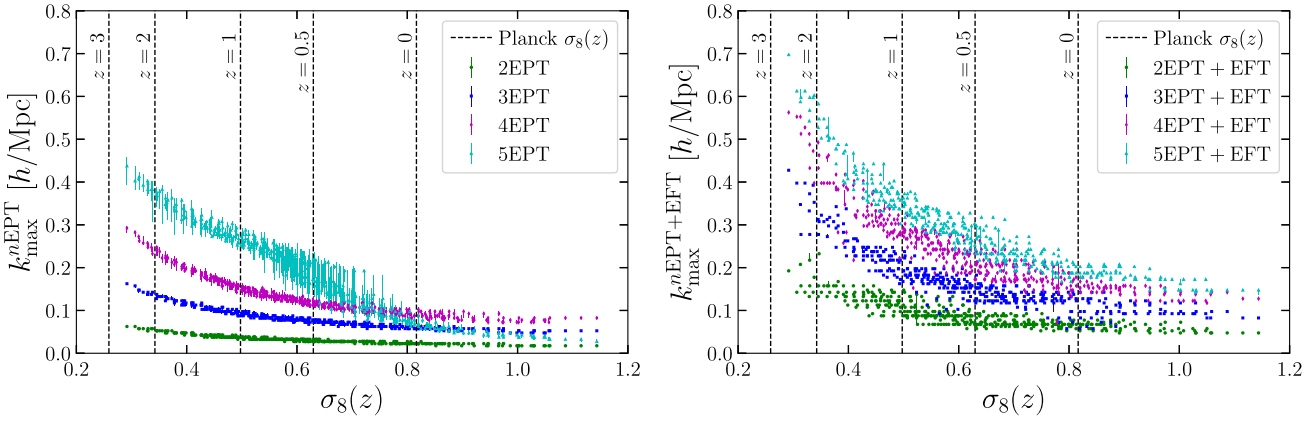

FIG. 4. (*Left*) The anticorrelation between the $k_{\rm max}$, the maximum wave number where *n*EPT matches N-body result to 1% accuracy, of *n*EPT and $\sigma_8(z)$ for Dark-Quest simulation's all 20 cosmologies at 21 redshifts from $z = 0$ to $z = 1.48$. The error bars show the range of $k_{\rm max}$ with varying UV cutoff between $(1.26, 2.14)$ h/Mpc. The dashed lines indicate the value of $\sigma_8(z)$ in *Planck* cosmology at redshifts $z = 0$, 0.5, 1, 1.5, 2, 3. (*Right*) The same as the left panel but for the *n*EPT power spectrum with EFT correction in Eq. (10).

V. CONCLUSION

In this paper, we present a novel *n*EPT resummation scheme and show that the *n*EPT outperforms one-loop and two-loop SPT as well as two-loop results of the RegPT+ and the IR-resummed EFT without employing any free parameters. The resummation scheme also offers well-regulated convergence behavior at each successive n, bypassing the pathological behavior shown in SPT.

To be a successful theory for modeling observed galaxy clustering, the *n*EPT still needs to incorporate the galaxy bias and the redshift-space distortion, but we anticipate that *n*EPT must still thrive, at the very least, by following the prescriptions in SPT and EFTofLSS. However, taking advantage of having both density and velocity at each grid point, one can directly implement the nonlinear redshift-space distortion mapping to improve the modeling accuracy further [77]. Upon the addition of galaxy bias and redshift-space distortion, the field-level modeling with *n*EPT will be a powerful data-analysis tool for future high-redshift galaxy surveys.

Finally, while we have only demonstrated the accuracy of the *n*EPT scheme, a more in-depth theoretical study of the underlying reason for such behavior is desired.

ACKNOWLEDGMENTS

D. J. is supported by KIAS Individual Grant No. PG088301 at the Korea Institute for Advanced Study. This work was supported in part by MEXT/JSPS KAKENHI Grants No. JP19H00677 (T. N.), No. JP20H05861, No. JP21H01081 (A. T. and T. N.), No. JP21J00011, No. JP22K14036 (K. O.), and No. JP22K03634 (T. N.). We also acknowledge financial support from Japan Science and Technology Agency (JST) AIP Acceleration Research Grant No. JP20317829 (A. T. and T. N.). Numerical computations were carried out at the ROAR supercomputer at Penn State University, Yukawa Institute Computer Facility, and Cray XC50 at Center for Computational Astrophysics, National Astronomical Observatory of Japan.

[1] C. L. Bennett *et al.*, Nine-year Wilkinson microwave anisotropy probe (WMAP) observations: Final maps and results, Astrophys. J. Suppl. Ser. **208**, 20 (2013).
[2] N. Aghanim, Y. Akrami, F. Arroja, M. Ashdown, J. Aumont, C. Baccigalupi, M. Ballardini, A. J. Banday, R. Barreiro, N. Bartolo *et al.*, Planck 2018 results I. Overview and the cosmological legacy of Planck, Astron. Astrophys. **641**, A1 (2020).
[3] M. Colless *et al.*, The 2dF Galaxy Redshift Survey: Spectra and redshifts, Mon. Not. R. Astron. Soc. **328**, 1039 (2001).
[4] K. Abazajian, J. K. Adelman-McCarthy, M. A. Agüeros, S. S. Allam, S. F. Anderson, J. Annis, N. A. Bahcall, I. K. Baldry *et al.*, The First Data Release of the Sloan Digital Sky Survey, Astron. J. **126**, 2081 (2003).
[5] M. J. Drinkwater *et al.*, The WiggleZ Dark Energy Survey: Survey design and first data release, Mon. Not. R. Astron. Soc. **401**, 1429 (2010).
[6] K. S. Dawson, D. J. Schlegel, C. P. Ahn, S. F. Anderson, É. Aubourg, S. Bailey, R. H. Barkhouser, J. E. Bautista, A. Beifiori, A. A. Berlind, V. Bhardwaj, D. Bizyaev, C. H. Blake *et al.*, The baryon oscillation spectroscopic survey of SDSS-III, Astron. J. **145**, 10 (2013).
[7] K. S. Dawson, J.-P. Kneib, W. J. Percival, S. Alam, F. D. Albareti, S. F. Anderson, E. Armengaud, É. Aubourg, S. Bailey, J. E. Bautista, A. A. Berlind, M. A. Bershady, F. Beutler *et al.*, The SDSS-IV extended baryon oscillation spectroscopic survey: Overview and early data, Astron. J. **151**, 44 (2016).
[8] H. Hildebrandt *et al.*, KiDS-450: Cosmological parameter constraints from tomographic weak gravitational lensing, Mon. Not. R. Astron. Soc. **465**, 1454 (2017).
[9] T. M. C. Abbott, F. B. Abdalla, A. Alarcon, J. Aleksić, S. Allam, S. Allen, A. Amara, J. Annis, J. Asorey, S. Avila, D. Bacon, E. Balbinot, M. Banerji, N. Banik, W. Barkhouse, M. Baumer *et al.*, Dark Energy Survey year 1 results: Cosmological constraints from galaxy clustering and weak lensing, Phys. Rev. D **98**, 043526 (2018).
[10] Planck Collaboration, N. Aghanim, Y. Akrami, M. Ashdown, J. Aumont, C. Baccigalupi, M. Ballardini, A. J. Banday, R. B. Barreiro, N. Bartolo, S. Basak, R. Battye, K. Benabed, J. P. Bernard, Bersanelli *et al.*, Planck 2018 results. VI. Cosmological parameters, Astron. Astrophys. **641**, A6 (2020).
[11] E. Lifshitz, Republication of: On the gravitational stability of the expanding universe, Gen. Relativ. Gravit. **49**, 18 (2017).
[12] P. J. E. Peebles and J. T. Yu, Primeval adiabatic perturbation in an expanding universe, Astrophys. J. **162**, 815 (1970).
[13] R. A. Sunyaev and Y. B. Zeldovich, Small-scale fluctuations of relic radiation, Astrophys. Space Sci. **7**, 3 (1970).
[14] J. R. Bond and G. Efstathiou, The statistics of cosmic background radiation fluctuations, Mon. Not. R. Astron. Soc. **226**, 655 (1987).
[15] G. Hinshaw *et al.*, Nine-year Wilkinson Microwave Anisotropy Probe (WMAP) Observations: Cosmological parameter results, Astrophys. J. Suppl. Ser. **208**, 19 (2013).
[16] G. J. Hill, K. Gebhardt, E. Komatsu, N. Drory, P. J. MacQueen, J. Adams, G. A. Blanc, R. Koehler, M. Rafal, M. M. Roth, A. Kelz, C. Gronwall, R. Ciardullo, and D. P. Schneider, The Hobby-Eberly Telescope Dark Energy Experiment (HETDEX): Description and early pilot survey results, ASP Conf. Ser. **399**, 115 (2008).

[17] M. Takada *et al.*, Extragalactic science, cosmology, and Galactic archaeology with the Subaru Prime Focus Spectrograph, Publ. Astron. Soc. Jpn. **66**, R1 (2014).
[18] M. Levi, C. Bebek, T. Beers, R. Blum, R. Cahn, D. Eisenstein, B. Flaugher, K. Honscheid, R. Kron, O. Lahav, P. McDonald, N. Roe, D. Schlegel, and representing the DESI Collaboration, The DESI Experiment, a whitepaper for Snowmass 2013, arXiv:1308.0847.
[19] LSST Dark Energy Science Collaboration, Large Synoptic Survey Telescope: Dark Energy Science Collaboration, arXiv:1211.0310.
[20] L. Amendola *et al.*, Cosmology and fundamental physics with the Euclid satellite, Living Rev. Relativity **21**, 2 (2018).
[21] R. Maartens, F. B. Abdalla, M. Jarvis, and M. G. Santos, Cosmology with the SKA—overview, *Proc. Sci.*, AASKA14 (2015) 016 [arXiv:1501.04076].
[22] O. Doré *et al.*, Cosmology with the SPHEREX all-sky spectral survey, arXiv:1412.4872.
[23] F. Beutler, C. Blake, M. Colless, D. H. Jones, L. Staveley-Smith, L. Campbell, Q. Parker, W. Saunders, and F. Watson, The 6dF Galaxy Survey: Baryon acoustic oscillations and the local Hubble constant, Mon. Not. R. Astron. Soc. **416**, 3017 (2011).
[24] S. Alam *et al.*, The clustering of galaxies in the completed SDSS-III Baryon Oscillation Spectroscopic Survey: Cosmological analysis of the DR12 galaxy sample, Mon. Not. R. Astron. Soc. **470**, 2617 (2017).
[25] A. J. Ross, L. Samushia, C. Howlett, W. J. Percival, A. Burden, and M. Manera, The clustering of the SDSS DR7 main Galaxy sample—I. A 4 per cent distance measure at $z = 0.15$, Mon. Not. R. Astron. Soc. **449**, 835 (2015).
[26] M. Shoji, D. Jeong, and E. Komatsu, Extracting angular diameter distance and expansion rate of the universe from two-dimensional galaxy power spectrum at high redshifts: Baryon acoustic oscillation fitting versus full modeling, Astrophys. J. **693**, 1404 (2009).
[27] O. H. E. Philcox, M. M. Ivanov, M. Simonović, and M. Zaldarriaga, Combining full-shape and BAO analyses of galaxy power spectra: A 1.6% CMB-independent constraint on H_0, J. Cosmol. Astropart. Phys. 05 (2020) 032.
[28] Y. Kobayashi, T. Nishimichi, M. Takada, and H. Miyatake, Full-shape cosmology analysis of the SDSS-III BOSS galaxy power spectrum using an emulator-based halo model: A 5% determination of σ_8, Phys. Rev. D **105**, 083517 (2022).
[29] J. Lesgourgues and S. Pastor, Massive neutrinos and cosmology, Phys. Rep. **429**, 307 (2006).
[30] O. H. E. Philcox and M. M. Ivanov, BOSS DR12 full-shape cosmology: ΛCDM constraints from the large-scale galaxy power spectrum and bispectrum monopole, Phys. Rev. D **105**, 043517 (2022).
[31] K. Heitmann, D. Bingham, E. Lawrence, S. Bergner, S. Habib, D. Higdon, A. Pope, R. Biswas, H. Finkel, N. Frontiere, and S. Bhattacharya, The Mira-Titan Universe: Precision predictions for dark energy surveys, Astrophys. J. **820**, 108 (2016).
[32] J. DeRose, R. H. Wechsler, J. L. Tinker, M. R. Becker, Y.-Y. Mao, T. McClintock, S. McLaughlin, E. Rozo, and Z. Zhai, The AEMULUS Project. I. Numerical simulations for precision cosmology, Astrophys. J. **875**, 69 (2019).
[33] T. Nishimichi, M. Takada, R. Takahashi, K. Osato, M. Shirasaki, T. Oogi, H. Miyatake, M. Oguri, R. Murata, Y. Kobayashi, and N. Yoshida, Dark quest. I. Fast and accurate emulation of halo clustering statistics and its application to galaxy clustering, Astrophys. J. **884**, 29 (2019).
[34] R. E. Angulo, M. Zennaro, S. Contreras, G. Aricò, M. Pellejero-Ibañez, and J. Stücker, The BACCO simulation project: Exploiting the full power of large-scale structure for cosmology, Mon. Not. R. Astron. Soc. **507**, 5869 (2021).
[35] S. Tassev, M. Zaldarriaga, and D. J. Eisenstein, Solving large scale structure in ten easy steps with COLA, J. Cosmol. Astropart. Phys. 06 (2013) 036.
[36] P. Monaco, E. Sefusatti, S. Borgani, M. Crocce, P. Fosalba, R. K. Sheth, and T. Theuns, An accurate tool for the fast generation of dark matter halo catalogues, Mon. Not. R. Astron. Soc. **433**, 2389 (2013).
[37] F. S. Kitaura and S. Hess, Cosmological structure formation with augmented Lagrangian perturbation theory, Mon. Not. R. Astron. Soc. **435**, L78 (2013).
[38] C.-H. Chuang, F.-S. Kitaura, F. Prada, C. Zhao, and G. Yepes, EZmocks: Extending the Zel'dovich approximation to generate mock galaxy catalogues with accurate clustering statistics, Mon. Not. R. Astron. Soc. **446**, 2621 (2015).
[39] S. He, Y. Li, Y. Feng, S. Ho, S. Ravanbakhsh, W. Chen, and B. Póczos, Learning to predict the cosmological structure formation, Proc. Natl. Acad. Sci. U.S.A. **116**, 13825 (2019).
[40] F. Villaescusa-Navarro *et al.*, The CAMELS Project: Cosmology and astrophysics with machine-learning simulations, Astrophys. J. **915**, 71 (2021).
[41] F. Bernardeau, S. Colombi, E. Gaztañaga, and R. Scoccimarro, Large-scale structure of the Universe and cosmological perturbation theory, Phys. Rep. **367**, 1 (2002).
[42] D. Jeong and E. Komatsu, Perturbation theory reloaded: Analytical calculation of nonlinearity in baryonic oscillations in the real-space matter power spectrum, Astrophys. J. **651**, 619 (2006).
[43] M. White, The Zel'dovich approximation, Mon. Not. R. Astron. Soc. **439**, 3630 (2014).
[44] S.-F. Chen, Z. Vlah, E. Castorina, and M. White, Redshift-space distortions in Lagrangian perturbation theory, J. Cosmol. Astropart. Phys. 03 (2021) 100.
[45] D. Baumann, A. Nicolis, L. Senatore, and M. Zaldarriaga, Cosmological non-linearities as an effective fluid, J. Cosmol. Astropart. Phys. 07 (2012) 051.
[46] J. J. M. Carrasco, M. P. Hertzberg, and L. Senatore, The effective field theory of cosmological large scale structures, J. High Energy Phys. 09 (2012) 082.
[47] M. P. Hertzberg, Effective field theory of dark matter and structure formation: Semianalytical results, Phys. Rev. D **89**, 043521 (2014).
[48] M. Crocce and R. Scoccimarro, Renormalized cosmological perturbation theory, Phys. Rev. D **73**, 063519 (2006).
[49] M. Crocce and R. Scoccimarro, Memory of initial conditions in gravitational clustering, Phys. Rev. D **73**, 063520 (2006).
[50] M. Crocce and R. Scoccimarro, Nonlinear evolution of baryon acoustic oscillations, Phys. Rev. D **77**, 023533 (2008).
[51] P. Valageas, Large-N expansions applied to gravitational clustering, Astron. Astrophys. **465**, 725 (2007).

[52] A. Taruya and T. Hiramatsu, A closure theory for nonlinear evolution of cosmological power spectra, Astrophys. J. **674**, 617 (2008).
[53] A. Taruya, T. Nishimichi, S. Saito, and T. Hiramatsu, Non-linear evolution of baryon acoustic oscillations from improved perturbation theory in real and redshift spaces, Phys. Rev. D **80**, 123503 (2009).
[54] T. Matsubara, Resumming cosmological perturbations via the Lagrangian picture: One-loop results in real space and in redshift space, Phys. Rev. D **77**, 063530 (2008).
[55] M. Pietroni, Flowing with time: A new approach to non-linear cosmological perturbations, J. Cosmol. Astropart. Phys. 10 (2008) 036.
[56] F. Bernardeau, M. Crocce, and R. Scoccimarro, Multipoint propagators in cosmological gravitational instability, Phys. Rev. D **78**, 103521 (2008).
[57] F. Bernardeau, M. Crocce, and R. Scoccimarro, Constructing regularized cosmic propagators, Phys. Rev. D **85**, 123519 (2012).
[58] D. Blas, M. Garny, M. M. Ivanov, and S. Sibiryakov, Time-sliced perturbation theory for large scale structure I: General formalism, J. Cosmol. Astropart. Phys. 07 (2016) 052.
[59] D. Blas, M. Garny, M. M. Ivanov, and S. Sibiryakov, Time-sliced perturbation theory II: Baryon acoustic oscillations and infrared resummation, J. Cosmol. Astropart. Phys. 07 (2016) 028.
[60] A. Taruya, F. Bernardeau, T. Nishimichi, and S. Codis, Direct and fast calculation of regularized cosmological power spectrum at two-loop order, Phys. Rev. D **86**, 103528 (2012).
[61] K. Osato, T. Nishimichi, F. Bernardeau, and A. Taruya, Perturbation theory challenge for cosmological parameters estimation: Matter power spectrum in real space, Phys. Rev. D **99**, 063530 (2019).
[62] M. Schmittfull, Z. Vlah, and P. McDonald, Fast large scale structure perturbation theory using one-dimensional fast Fourier transforms, Phys. Rev. D **93**, 103528 (2016).
[63] J. E. McEwen, X. Fang, C. M. Hirata, and J. A. Blazek, FAST-PT: A novel algorithm to calculate convolution integrals in cosmological perturbation theory, J. Cosmol. Astropart. Phys. 09 (2016) 015.
[64] X. Fang, J. A. Blazek, J. E. McEwen, and C. M. Hirata, FAST-PT II: An algorithm to calculate convolution integrals of general tensor quantities in cosmological perturbation theory, J. Cosmol. Astropart. Phys. 02 (2017) 030.
[65] M. Simonović, T. Baldauf, M. Zaldarriaga, J. J. Carrasco, and J. A. Kollmeier, Cosmological perturbation theory using the FFTLog: Formalism and connection to QFT loop integrals, J. Cosmol. Astropart. Phys. 04 (2018) 030.
[66] K. Osato, T. Nishimichi, A. Taruya, and F. Bernardeau, Implementing spectra response function approaches for fast calculation of power spectra and bispectra, Phys. Rev. D **104**, 103501 (2021).
[67] A. J. S. Hamilton, Uncorrelated modes of the non-linear power spectrum, Mon. Not. R. Astron. Soc. **312**, 257 (2000).
[68] T. Nishimichi, F. Bernardeau, and A. Taruya, Moving around the cosmological parameter space: A nonlinear power spectrum reconstruction based on high-resolution cosmic responses, Phys. Rev. D **96**, 123515 (2017).
[69] M. Schmittfull and Z. Vlah, Reducing the two-loop large-scale structure power spectrum to low-dimensional, radial integrals, Phys. Rev. D **94**, 103530 (2016).
[70] T. Baldauf, E. Schaan, and M. Zaldarriaga, On the reach of perturbative methods for dark matter density fields, J. Cosmol. Astropart. Phys. 03 (2016) 007.
[71] A. Taruya, T. Nishimichi, and D. Jeong, Grid-based calculation for perturbation theory of large-scale structure, Phys. Rev. D **98**, 103532 (2018).
[72] M. Schmittfull, M. Simonović, V. Assassi, and M. Zaldarriaga, Modeling biased tracers at the field level, Phys. Rev. D **100**, 043514 (2019).
[73] C. Modi, M. White, A. Slosar, and E. Castorina, Reconstructing large-scale structure with neutral hydrogen surveys, J. Cosmol. Astropart. Phys. 11 (2019) 023.
[74] A. Taruya, T. Nishimichi, and D. Jeong, Covariance of the matter power spectrum including the survey window function effect: N -body simulations versus fifth-order perturbation theory on grids, Phys. Rev. D **103**, 023501 (2021).
[75] F. Schmidt, An n-th order Lagrangian forward model for large-scale structure, J. Cosmol. Astropart. Phys. 04 (2021) 033.
[76] M. Schmittfull, M. Simonović, M. M. Ivanov, O. H. E. Philcox, and M. Zaldarriaga, Modeling galaxies in redshift space at the field level, J. Cosmol. Astropart. Phys. 05 (2021) 059.
[77] A. Taruya, T. Nishimichi, and D. Jeong, Grid-based calculations of redshift-space matter fluctuations from perturbation theory: UV sensitivity and convergence at the field level, Phys. Rev. D **105**, 103507 (2022).
[78] A. Andrews, J. Jasche, G. Lavaux, and F. Schmidt, Bayesian field-level inference of primordial non-Gaussianity using next-generation galaxy surveys, Mon. Not. R. Astron. Soc. **520**, 5746 (2023).
[79] E. Komatsu, J. Dunkley, M. R. Nolta, C. L. Bennett, B. Gold, G. Hinshaw, N. Jarosik, D. Larson, M. Limon, L. Page, D. N. Spergel, M. Halpern, R. S. Hill, A. Kogut, S. S. Meyer, G. S. Tucker, J. L. Weiland, E. Wollack, and E. L. Wright, Five-Year Wilkinson Microwave Anisotropy Probe Observations: Cosmological Interpretation, Astrophys. J. Suppl. Ser. **180**, 330 (2009).
[80] T. Nishimichi, M. Takada, R. Takahashi, K. Osato, M. Shirasaki, T. Oogi, H. Miyatake, M. Oguri, R. Murata, Y. Kobayashi, and N. Yoshida, Dark quest. I. Fast and accurate emulation of halo clustering statistics and its application to galaxy clustering, Astrophys. J. **884**, 29 (2019).
[81] P. A. R. Ade *et al.* (Planck Collaboration), Planck 2015 results. XIII. Cosmological parameters, Astron. Astrophys. **594**, A13 (2016).
[82] Y. P. Jing, Correcting for the alias effect when measuring the power spectrum using a fast Fourier transform, Astrophys. J. **620**, 559 (2005).
[83] E. Sefusatti, M. Crocce, R. Scoccimarro, and H. M. P. Couchman, Accurate estimators of correlation functions in Fourier space, Mon. Not. R. Astron. Soc. **460**, 3624 (2016).
[84] D. Jeong, Cosmology with high ($z > 1$) redshift galaxy surveys, Ph.D. thesis, University of Texas, Austin, 2010.

[85] R. Takahashi, N. Yoshida, T. Matsubara, N. Sugiyama, I. Kayo, T. Nishimichi, A. Shirata, A. Taruya, S. Saito, K. Yahata, and Y. Suto, Simulations of baryon acoustic oscillations—I. Growth of large-scale density fluctuations, Mon. Not. R. Astron. Soc. **389**, 1675 (2008).

[86] L. Senatore and M. Zaldarriaga, The IR-resummed effective field theory of large scale structures, J. Cosmol. Astropart. Phys. 02 (2015) 013.

[87] Z. Vlah, U. Seljak, M. Yat Chu, and Y. Feng, Perturbation theory, effective field theory, and oscillations in the power spectrum, J. Cosmol. Astropart. Phys. 03 (2016) 057.